Shear Viscosity of a Unitary Fermi Gas Near the Superfluid Phase Transition

J. A. Joseph, E. Elliott, and J. E. Thomas

Phys. Rev. Lett. **115**, 020401 — Published 6 July 2015

DOI: 10.1103/PhysRevLett.115.020401

Shear viscosity of a unitary Fermi gas near the superfluid phase transition

J. A. Joseph[1], E. Elliott[1,2], and J. E. Thomas[1]
[1]*Department of Physics, North Carolina State University, Raleigh, NC 27695, USA and*
[2]*Department of Physics, Duke University, Durham, NC 27708, USA*
(Dated: June 15, 2015)

We measure the shear viscosity for a resonantly interacting Fermi gas as a function of temperature from nearly the ground state through the superfluid phase transition into the high temperature regime. Further, we demonstrate an iterative method to estimate the *local* shear viscosity coefficient $\alpha_S(\theta)$ versus reduced temperature θ from the cloud-averaged measurements $\langle\alpha_S\rangle$, and compare α_S to several microscopic theories. We find that α_S reveals features that were previously hidden in $\langle\alpha_S\rangle$.

Condensates of bosons or fermion pairs exhibit nearly frictionless hydrodynamic flow near and below a critical temperature, T_c, which is a defining and striking macroscopic property of superfluids. Just above T_c, where the fluid is normal, a regime of extremely small, but finite, shear viscosity is observed. A universal lower bound for the ratio of shear viscosity to entropy density, $\hbar/(4\pi\, k_B)$, is conjectured for this normal fluid regime [1]. Below T_c, the behavior of the shear viscosity of bosonic and fermionic fluids is quite different. In bosonic ^{4}He [2], there is an increase in the shear viscosity as the temperature decreases below T_c, which is believed to arise from single particle bosonic excitations that couple to the collective (Nambu-Goldstone) modes [3, 4]. In fermionic ^{3}He [5], the shear viscosity decreases rapidly to zero as the temperature decreases below T_c, most likely as a result of the suppression of fermionic excitations at low temperatures [4].

An optically trapped, ultra-cold Fermi gas of atoms tuned near a collisional (Feshbach) resonance provides a new paradigm for the study of shear viscosity in quantum fluids [6, 7], enabling experimental access not only to Bose and Fermi superfluid systems, but also to a resonant, universal regime, where the gas has both fermionic and bosonic properties. Near a Feshbach resonance [8, 9], a bias magnetic field applied to a trapped cloud tunes the interaction strength between atoms in two different hyperfine states, denoted spin-up and spin-down. Well above resonance, atoms in different spin states are weakly attractive, and the system can be described by Bardeen-Cooper-Schrieffer (BCS) theory. Well below resonance, pairs of spin-up and spin-down atoms are tightly bound into weakly repulsive molecular bosons, where Bose-Einstein condensate (BEC) theory is applicable. On resonance, there exists a very strongly interacting state of matter, the unitary or universal Fermi gas (UFG), which exhibits scale-invariant hydrodynamic expansion [10].

We report the measurement of the shear viscosity of a UFG as a function of temperature below the superfluid transition temperature, testing the degree to which its transport properties align with those of Bose and Fermi quantum fluids. By observing the expansion of a cigar-shaped cloud, we first obtain the shear viscosity averaged over the density profile. In this cloud-averaged data, we observe a rapid decrease in the shear viscosity as the temperature is reduced below T_c. We then demonstrate a method for inverting the cloud-averaged viscosity data to estimate the *local* shear viscosity as a function of reduced temperature, revealing features that were previously hidden in the cloud-averages. This inverted data for the local shear viscosity is compared to recent theories of the shear viscosity for a UFG in the transition region [4, 11–17], which differ in the predicted contributions of pair correlations, fermionic excitations, and bosonic excitations at low temperature. Using the measured local shear viscosity and the measured local entropy density [18], we also determine the local ratio of the shear viscosity to the entropy density, which is compared to the universal lower bound conjectured by Kovtun, Son, and Starinets [1].

In the experiments, a Fermi gas of ^{6}Li atoms is prepared in a 50-50 mixture of the two lowest hyperfine states and confined in a cigar-shaped optical trap with an elliptical transverse profile. The trap oscillation frequencies are $(\omega_x, \omega_y, \omega_z) = 2\pi \times [2210(4), 830(2), 64(0.5)]$ Hz. The cloud is tuned near a broad Feshbach resonance and cooled by evaporation [19] to nearly the ground state. The final temperature of the gas is controlled by altering the optical trap lowering curve used for evaporation.

The cloud is abruptly released from the trap and imaged from two orthogonal directions at a time t after release to determine the cloud radii $\sigma_i(t)$ in all three directions, $i = x, y, z$. There is evidence that the superfluid and normal fluid components of a UFG move together in hydrodynamic expansion [10], which is consistent with the existence of exact scaling solutions for a two-fluid model of the collective modes [20]. We therefore assume that the cloud radii expand according to a single-fluid model, where $\sigma_i(t) = \sigma_i(0)\, b_i(t)$. The hydrodynamic expansion factors $b_i(t)$ obey universal evolution equations that include viscous forces and heating [10, 21]. Using the known trap parameters, the cloud radii data are fit using the cloud-averaged shear viscosity coefficient $\langle\alpha_S\rangle$ as a free parameter. The initial cloud radii $\sigma_i(0)$ and $\langle\alpha_S\rangle$ are self-consistently determined from the transverse aspect ratio $\sigma_x(t)/\sigma_y(t)$ using only *one* expansion time t for one measurement [21]. For the new data presented in

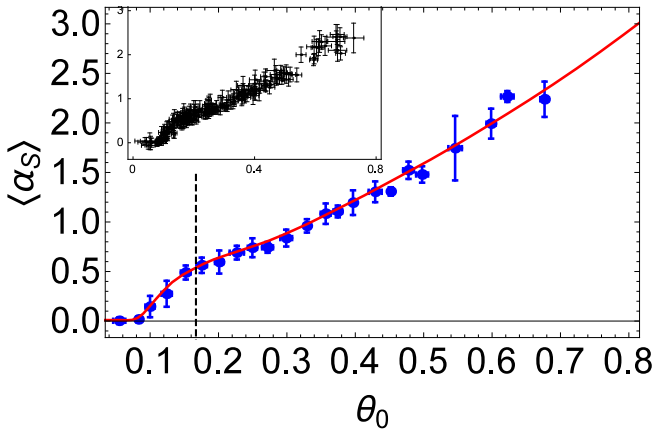

FIG. 1. Trap-averaged shear viscosity coefficient $\langle\alpha_S\rangle$, where the shear viscosity is $\eta = \alpha_S\,\hbar n$. The solid blue points show the $\langle\alpha_S\rangle$ data versus reduced temperature θ_0 at the trap center, after binning the raw data (inset) in θ_0. The vertical dashed line denotes the critical temperature at the trap center $\theta_c = 0.167(13)$ [18]. The red solid line is obtained by integrating $\alpha_S(\theta)$, which is estimated from the $\langle\alpha_S\rangle$ data using an image processing algorithm.

this paper, which extends to very low temperature, this method greatly increases the temperature resolution, see Fig. 1 (inset).

The measured shear viscosity coefficient is related to the shear viscosity, η, which has a dimension of momentum/area, and hence is given in natural units of $\hbar\,n$, where $n = n(\mathbf{r})$ is the local density. A local shear viscosity coefficient α_S is then defined by $\eta \equiv \alpha_S\,\hbar\,n$ [6]. As noted above, the measurements determine a cloud-averaged shear viscosity coefficient $\langle\alpha_S\rangle$, which is defined by

$$\langle\alpha_S\rangle \equiv \frac{1}{N\hbar}\int d^3\mathbf{r}\,\eta = \frac{1}{N}\int d^3\mathbf{r}\,n\,\alpha_S(\theta), \qquad (1)$$

where N is the total number of atoms. As shown previously for a UFG, $\alpha_S(\theta)$ is a function only of the local reduced temperature $\theta \equiv T/T_F(n)$, where $T_F(n)$ is the local Fermi temperature. Further, $\langle\alpha_S\rangle$ is temporally constant as the cloud expands, i.e., it is equal to the cloud-averaged initial value with $n \to n(\mathbf{r}, t = 0)$ [6, 7, 21].

Fig. 1 shows the trap-averaged shear viscosity coefficient $\langle\alpha_S\rangle$ as a function of the reduced temperature at the center of the trap $\theta_0 = T/T_F(n_0)$, where $n_0 \equiv n(\mathbf{r} = 0)$. Temperature is determined from the measured cloud profile. The measured trap potential [22] and the equation of state measured by Ku et al., [18] are used to determine the local density as a function of reduced temperature at the cloud center, θ_0, i.e., $n(r, \theta_0)$. This relates the measured cloud profile to θ_0.

We now show that the trap-averaged data of Fig. 1 for $\langle\alpha_S\rangle$ versus θ_0 can be inverted to estimate the *local* shear viscosity coefficient $\alpha_S(\theta)$ as a function of the local reduced temperature $\theta = T/T_F(n)$. For a single measurement of $\langle\alpha_S\rangle$ at θ_0, the reduced temperature $\theta = \theta_0\,(n_0/n)^{2/3}$ has a minimum θ_0 at the trap center and increases as the density n decreases. Therefore, a single measurement contains information over a range of reduced temperatures, which enables an estimate of $\alpha_S(\theta)$ from the trap-averaged data, by using an Iterative Shrinking/Thresholding (IST) algorithm, a technique that is commonly used in imaging processing [23].

However, $\langle\alpha_S\rangle$ is formally divergent. For large θ, $\alpha_S(\theta) \to \alpha_{3/2}\,\theta^{3/2} \propto T^{3/2}/n$, where $\alpha_{3/2} = 45\pi^{3/2}/(64\sqrt{2}) \simeq 2.77$ [12]. Then, in the low density region, the integrand $n\,\alpha_S(\theta) = n_0\,\alpha_S(\theta_0)$ is independent of density. Fortunately, energy conservation assures that the integral must be finite and kinetic theory shows that the shear viscosity $\eta = \hbar\,n\,\alpha_S \to 0$ as the density vanishes [11].

In our data inversion procedure, we circumvent this problem using a simple approximation, which assures that the local shear viscosity scales properly as $T^{3/2}$ in the low density (but still hydrodynamic) part of the cloud. This is accomplished by experimentally determining a finite volume, which is bounded by a cut-off radius, R_c. We find R_c from $\langle\alpha_S\rangle$ data in the temperature region where $\langle\alpha_S\rangle$ has a universal $\theta_0^{3/2}$ dependence [6, 7, 21]. Using $\langle\alpha_S\rangle = c_0 + c_1\,\theta_0^{3/2}$ to fit the data yields $c_0 = 0.34(4)$ and $c_1 = 3.60(15)$ [24]. The cutoff radius R_c is then found from Eq. 1, which requires $\alpha_{3/2}\,4\pi R_c^3 n_0/(3N) = c_1$ [22, 24]. We assume a gaussian density profile, with central density $n_0 = N(\pi\frac{2}{3}\langle r^2\rangle)^{-3/2}$. Then we find $R_c = 0.98\,\langle r^2\rangle^{1/2}$ [24]. Here, $\langle r^2\rangle$ is the (temperature-dependent) mean square radius of the trapped cloud in *scaled* coordinates [22]. Making the simplest scale-invariant assumption, we take $R_c = \langle r^2\rangle^{1/2}$ at all temperatures [24].

Now we assume a piecewise representation of the local shear viscosity, using a discrete set of reduced temperatures θ_i, with $\alpha_S(\theta) = \alpha_i$ for $\theta_i \le \theta \le \theta_{i+1}$. Eq. 1 is then converted into a system of linear equations, with the j^{th} equation corresponding to the j^{th} measurement of the trap-averaged shear viscosity $\langle\alpha_S\rangle_j$ with a reduced temperature θ_{0j} at the trap center,

$$\langle\alpha_S\rangle_j = \sum_i C_{ji}\alpha_i$$
$$C_{ji} \equiv \int_{R_i(\theta_{0j})}^{R_{i+1}(\theta_{0j})} 4\pi r^2\,n(r, \theta_{0j})\,dr, \qquad (2)$$

For each θ_i, $(\theta_i/\theta_{0j})^{3/2} = n(0, \theta_{0j})/n(R_i, \theta_{0j})$ determines $R_i(\theta_{0j})$. We can write Eq. 2 in matrix form,

$$\langle\boldsymbol{\alpha_S}\rangle = \mathbf{C}\cdot\boldsymbol{\alpha}. \qquad (3)$$

The IST algorithm [23] removes high frequency noise associated with measurements, but leaves enough resolution to determine the smooth behavior and significant

transitions in the local shear viscosity [24]. Our implementation of the IST algorithm takes the form,

$$\boldsymbol{\alpha_{m+1}} = (1-\beta)\boldsymbol{\alpha_m} + \beta\Psi[\boldsymbol{\alpha_m} + \mathbf{C^T}(\langle\boldsymbol{\alpha}\rangle - \mathbf{C}\cdot\boldsymbol{\alpha_m})], \quad (4)$$

where m is the iteration number and $\boldsymbol{\alpha}_{m+1}$ is determined from the previous m-step, $\boldsymbol{\alpha}_m$. Here, $0 \leq \beta \leq 1$ is an adjustable parameter that determines the speed of convergence of the iterative process, $\mathbf{C^T}$ is the transpose of $\mathbf{C}$, and $\Psi(\mathbf{x})$ is a non-quadratic denoising function. We choose $\Psi(\mathbf{x})$ to be a three-point moving average. The local shear viscosity converges slowly from an initial seed $\boldsymbol{\alpha}_0$, which we take to be the high temperature approximation for the local shear viscosity, discussed above, $2.77\,\theta_i^{3/2}$.

For our viscosity data, Eq. 4 is robust in the choice of β. We monitor the change in $\boldsymbol{\alpha}$ as a function of iteration number m in order to determine convergence. For $\boldsymbol{\alpha}$ shown in this paper, where $\beta = 0.1$, the IST algorithm converges after $m = 50$ iterations. The supplemental material provides a review of our implementation of the IST algorithm [24].

Fig. 2 shows the local shear viscosity coefficient $\alpha_S(\theta)$ obtained using Eq. 4 and the seed function $2.77\,\theta^{3/2}$. For large θ, the local shear viscosity converges to the two-body Boltzmann equation limit $\alpha = 2.77\,\theta^{3/2}$ [12] by construction, i.e., by our choice of $R_c(\theta_0)$. As θ is decreased to $\theta \simeq 1$, $\alpha_S(\theta)$ rises above the high T prediction. Since the viscosity is inversely proportional to the collision rate in the two-body limit, this result is consistent with a decreasing collision rate arising from Pauli blocking as the gas starts to become degenerate. Above the critical temperature, we see that α is larger than $2.77\,\theta^{3/2}$. As a consistency check, we integrate the $\alpha_S(\theta)$ determined by the IST algorithm over the cloud volume up to R_c, using Eq. 1. This yields the red curve in Fig. 1, which fits the measured trap-averaged viscosity coefficients with a normalized $\widetilde{\chi}^2 = 1.0$.

Fig. 3 shows $\alpha_S(\theta)$ in the low temperature regime, which is compared to microscopic theories. We observe that $\alpha_S(\theta)$ rises with increasing temperature much more sharply than the cloud-average $\langle\alpha_S\rangle$ of Fig. 1. The measured maximum slope $\alpha_S'(\theta)$ may be limited by the resolution of our inversion procedure, as explored in more detail in the supplemental material [24]. Below T_c, our estimated local shear viscosity is in remarkably good agreement with theoretical prediction based generally on pseudogap-BCS theory, which includes contributions from non-condensed pairs [4]. The QMC [16] result captures the qualitative shape, but is closer to the two-body limit than our estimate near the superfluid transition. Predictions using a diagrammatic approach, starting from the exact Kubo formula [15], are well above the two-body limit, closer to our estimates, and in good agreement with the estimated slope of $\alpha(\theta)$ above $\theta = 0.3$. At the very lowest temperatures measured, the estimated α_S is consistent with zero. We find

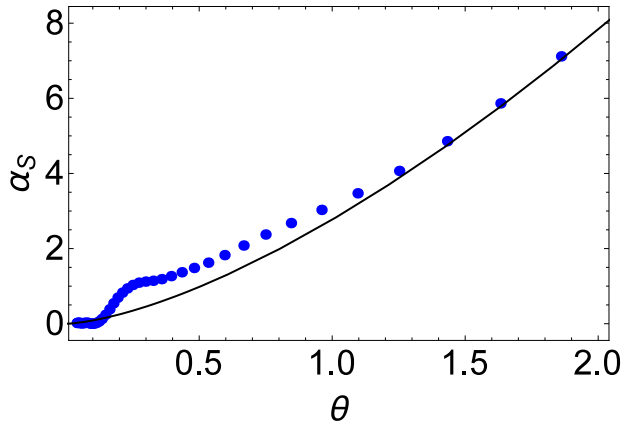

FIG. 2. Local shear viscosity coefficient α_S (blue dots) versus reduced temperature $\theta = T/T_F(n)$. The prediction from the two-body Boltzmann equation [12] $2.77\theta^{3/2}$ (black curve) is used as a seed function to initialize the iteration procedure and as a constraint at large θ.

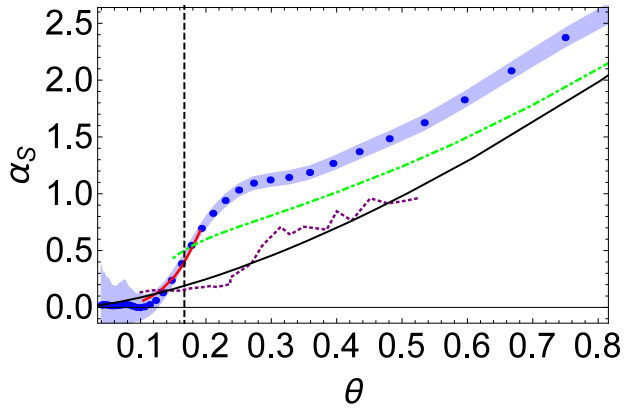

FIG. 3. Extracted local shear viscosity coefficient α_S (blue dots) versus reduced temperature $\theta = T/T_F(n)$ near the superfluid transition temperature, where the local shear viscosity is $\eta = \alpha_S(\theta)\hbar n$. The vertical dashed line denotes the critical temperature $\theta_c = 0.167(13)$ [18]. Blue bands denote the standard error corresponding to the statistical uncertainty in $\langle\alpha_S\rangle$; Red solid line from Guo et al., Ref. [4]; Green dotted curve from Enss et al, Ref. [15]; Purple dot-dashed curve from Wlazlowski et al., Ref. [16]; Black-solid line prediction from kinetic theory $\alpha_S = 2.77\,\theta^{3/2}$ [12].

the interesting result that the slope $\alpha_S'(\theta)$ of the inverted data has a peak at the superfluid transition temperature, Fig. 4, which is robust with respect to our choice of parameters in implementing the IST algorithm. This is reasonable, as we expect that the superfluid fraction varies most strongly near θ_c.

Next, we determine the ratio of the local shear viscosity to the local entropy density, using the entropy data of Ref. [18]. The ratio is compared to the lower bound conjectured by Kovtun, Son, and Starinets [1], as shown

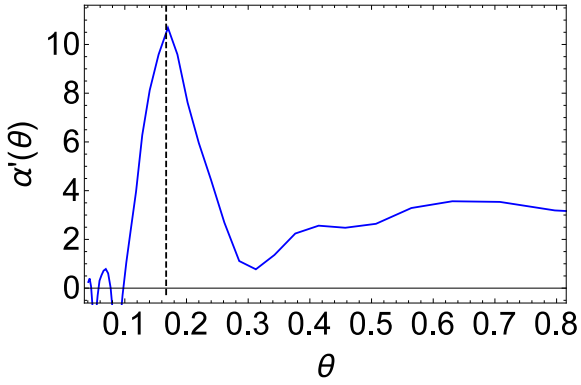

FIG. 4. Slope of the shear viscosity coefficient α_S versus reduced temperature θ, showing a peak at T_c. The vertical dashed line denotes the critical reduced temperature.

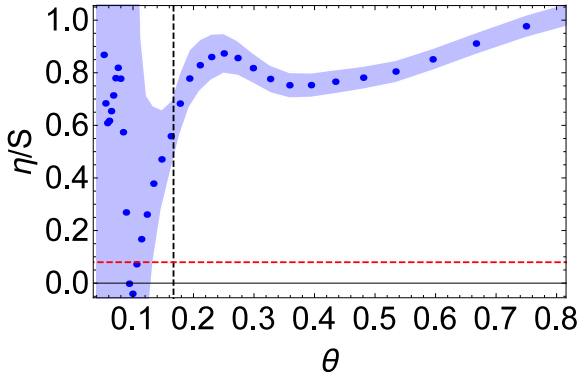

FIG. 5. Ratio of shear viscosity η to the entropy density s, in units of $\hbar/k_B$, versus reduced temperature $\theta = T/T_F(n)$. Blue dots are the ratio of the local shear viscosity, obtained from our matrix inversion method, to the entropy density measured in Ref. [18]. Blue bands denote the standard error for quadratically combining the statistical uncertainties in $\langle\alpha_S\rangle$ and in s. The vertical dashed line denotes the critical reduced temperature and the horizontal dashed line at $1/(4\pi)$ indicates the KSS lower bound [1].

in Fig. 5. We find that the ratio has a relatively weak dependance on θ for a range of temperature above the superfluid transition temperature, a shallow minimum for $\theta \approx 0.4$ in the normal fluid regime, where of $\eta/S = 0.5$, $\simeq 6$ times the predicted lower bound [1]. These features are in qualitative agreement with the predictions of Enss et al, Ref. [15]. In addition, there appears to be a minimum in the ratio below T_c and an upturn in the ratio as $T \to 0$. However, as both the entropy and the viscosity are rapidly approaching zero in this region, the error associated with both of the measured quantities does not permit an unambiguous determination.

We have presented a precision measurement of the cloud-averaged shear viscosity as a function of reduced temperature at the cloud center $\langle\alpha_S\rangle$, from well below the superfluid phase transition to the high temperature limit. We observe a rapid decrease in the measured shear viscosity below T_c, which suggests that the universal shear viscosity of a unitary Fermi gas is closer in character to that of fermionic ^{3}He than to bosonic ^{4}He. Further, we estimate the local shear viscosity coefficient $\alpha_S(\theta)$ from cloud-averaged data using an image processing method. We assume that the viscous forces in the expanding cloud act within a finite effective radius R_c, which we experimentally determine to assure convergence to the two-body Boltzmann equation limit at high temperature. Although determination of the systematic uncertainty in the magnitude of $\alpha_S(\theta)$ arising from this choice of R_c is difficult [24], our estimated local shear viscosity coefficient $\alpha_S(\theta)$ already reveals qualitative features that are hidden in $\langle\alpha_S\rangle$, and can be directly compared to predictions for homogenous systems.

This research is supported by the Physics Division of the National Science Foundation (Quantum hydrodynamics in interacting Fermi gases) and by the Division of Materials Science and Engineering, the Office of Basic Energy Sciences, Office of Science, U.S. Department of Energy (Thermodynamics in strongly correlated Fermi gases). Additional support has been provided by the Physics Divisions of the Army Research Office and the Air Force Office of Scientific Research. The authors are pleased to acknowledge M. Bluhm and T. Schäfer, North Carolina State University, for stimulating conversations and M. Gehm, Duke University, for suggesting the use of image processing methods.

[1] P. K. Kovtun, D. T. Son, and A. O. Starinets, Phys. Rev. Lett. **94**, 111601 (2005).
[2] A. D. B. Woods and A. C. H. Hallett, Canadian Journal of Physics **41**, 596 (1963).
[3] Q. Chen, J. Stajic, S. Tan, and K. Levin, Physics Reports **412**, 1 (2005).
[4] H. Guo, D. Wulin, C.-C. Chien, and K. Levin, Phys. Rev. Lett. **107**, 020403 (2011).
[5] T. Alvesalo, H. Collan, M. Loponen, O. Lounasmaa, and M. Veuro, Journal of Low Temperature Physics **19**, 1 (1975).
[6] C. Cao, E. Elliott, J. Joseph, H. Wu, J. Petricka, T. Schäfer, and J. E. Thomas, Science **331**, 58 (2011).
[7] C. Cao, E. Elliott, H. Wu, and J. E. Thomas, New J. Phys. **13**, 075007 (2011).
[8] M. Bartenstein, A. Altmeyer, S. Riedl, R. Geursen, S. Jochim, C. Chin, J. H. Denschlag, R. Grimm, A. Simoni, E. Tiesinga, C. J. Williams, and P. S. Julienne, Phys. Rev. Lett. **94**, 103201 (2005).
[9] G. Zürn, T. Lompe, A. N. Wenz, S. Jochim, P. S. Julienne, and J. M. Hutson, Phys. Rev. Lett. **110**, 135301 (2013).
[10] E. Elliott, J. A. Joseph, and J. E. Thomas, Phys. Rev. Lett. **112**, 040405 (2014).
[11] P. Massignan, G. M. Bruun, and H. Smith, Phys. Rev.

A **71**, 033607 (2005).
[12] G. M. Bruun and H. Smith, Phys. Rev. A **75**, 043612 (2007).
[13] G. Rupak and T. Schäfer, Phys. Rev. A **76**, 053607 (2007).
[14] E. Taylor and M. Randeria, Phys. Rev. A **81**, 053610 (2010).
[15] T. Enss, R. Haussmann, and W. Zwerger, Annals Phys. **326**, 770 (2011).
[16] G. Wlazłowski, P. Magierski, and J. E. Drut, Phys. Rev. Lett. **109**, 020406 (2012).
[17] G. Wlazłowski, P. Magierski, A. Bulgac, and K. J. Roche, Phys. Rev. A **88**, 013639 (2013).
[18] M. J. Ku, A. T. Sommer, L. W. Cheuk, and M. W. Zwierlein, Science **335**, 563 (2012).
[19] K. M. O'Hara, S. L. Hemmer, M. E. Gehm, S. R. Granade, and J. E. Thomas, Science **298**, 2179 (2002).
[20] Y.-H. Hou, L. P. Pitaevskii, and S. Stringari, Phys. Rev. A **87**, 033620 (2013).
[21] E. Elliott, J. A. Joseph, and J. E. Thomas, Phys. Rev. Lett. **113**, 020406 (2014).
[22] We transform to spherical symmetry in the usual way with scaled coordinates, $\bar{\omega}\tilde{x}_i \equiv \omega_i x_i$, where $\bar{\omega} \equiv (\omega_x\omega_y\omega_z)^{1/3}$, so that $r^2 = \sum_i \tilde{x}_i^2$, i.e., the effective trap potential energy is then a function of r. For a harmonic trap, $\sum_i m\omega_i^2\, x_i^2/2 = m\bar{\omega}^2\, r^2/2$.
[23] J. Bioucas-Dias and M. Figueiredo, IEEE Transactions on Image Processing **16**, 2992 (2007).
[24] See the online supplemental material for a detailed description of the iterative data inversion method, which includes Refs. [25, 26].
[25] J. E. Thomas, J. Kinast, and A. Turlapov, Phys. Rev. Lett. **95**, 120402 (2005).
[26] L. Luo and J. E. Thomas, J. Low Temp. Phys. **154**, 1 (2009).